Research Article

Humaira Yasmin*, Ali M. Mahnashi, Waleed Hamali, Showkat Ahmad Lone, Zehba Raizah, and Anwar Saeed*

A numerical analysis of the blood-based Casson hybrid nanofluid flow past a convectively heated surface embedded in a porous medium

https://doi.org/10.1515/phys-2023-0193
received November 15, 2023; accepted January 13, 2024

Abstract: The analysis of the fluid flow with the energy transfer across a stretching sheet has several applications in manufacturing developments such as wire drawing, hot rolling, metal extrusion, continuous casting, paper production, and glass fiber fabrication. The current examination presents the hybrid nanofluid flow past a convectively heated permeable sheet. The ferrous oxide (Fe_3O_4) and Gold (Au) nanoparticles have been dispersed in the blood. The significances of thermal radiation, inclined magnetic field, and space-dependent heat source have been observed in this work. The modeled equations are presented in the form of partial differential equations and reformed into the set of ordinary differential equations (ODEs) by using the similarity substitution. The Matlab built-in package (bvp4c) is employed to resolve the transform nonlinear set of ODEs. The significance of flow constraints *versus* the velocity and temperature profiles is demonstrated in the form of Figures and Tables. The numerical outcomes for the physical interest quantities are presented in tables. It has been perceived from the results that raising the angle of inclination from 0° to 90° reduces both the velocity and energy profile. The escalating values of Eckert number, constant heat source, and space-dependent heat source factor accelerate the temperature profile. The velocity and temperature distributions are very effective in the cases of hybrid nanofluid (Au–Fe_3O_4/blood) when compared to nanofluid (Au/blood). The skin friction and rate of heat transfer are very effective in the cases of hybrid nanofluid (Au–Fe_3O_4/blood) when compared to nanofluid (Au/blood).

Keywords: Hybrid nanofluid, MHD, space-dependent heat source, thermal-dependent heat source, porous media, Joule heating

Nomenclature

B_0	magnetic field (A/m)
Pr	Prandtl number
k	thermal conductivity (W m^{-1} K^{-1})
Rd	Radiation factor (J m^{-2} s^{-1})
Fe_3O_4	ferrous oxide nanoparticle
Ec	Eckert number
T_w	surface temperature (K)
C_{fx}	skin friction
M	magnetic factor (A/m)
$u_w(x) = ax$	stretching velocity (m/s)
C_p	specific heat (J kg^{-1} K^{-1})
Re	Reynolds number
Q_E	space-dependent heat source factor
Au	gold nanoparticle
Q_I	thermal-dependent heat source factor
B_T	thermal Biot number
Nu_x	Nusselt number

Greek symbols

σ	electrical conductivity (S/m)
ρ	density (kg/m^3)
$\lambda > 0$	stretching case of the sheet

* **Corresponding author: Humaira Yasmin**, Department of Basic Sciences, Preparatory Year, King Faisal University, Al Ahsa 31982, Saudi Arabia, e-mail: hhassain@kfu.edu.sa
* **Corresponding author: Anwar Saeed**, Department of Mathematics, Abdul Wali Khan University, Mardan, 23200, Khyber Pakhtunkhwa, Pakistan, e-mail: anwarsaeed769@gmail.com
Ali M. Mahnashi, Waleed Hamali: Department of Mathematics, College of Science, Jazan University, Jazan, Saudi Arabia
Showkat Ahmad Lone: Department of Basic Sciences, College of Science and Theoretical Studies, Saudi Electronic University, (Jeddah-M), Riyadh 11673, Saudi Arabia
Zehba Raizah: Department of Mathematics, College of Science, King Khalid University, Abha, Saudi Arabia

φ_1 volume fractions of iron oxide
φ_2 volume fractions of gold
$\lambda < 0$ shrinking case of the sheet

1 Introduction

The thermal transportation of various pure fluids can be enhanced by suspending tiny-sized particles like CNTs, metal ions, nano-powder, *etc*. Such fluids are nanofluids and are used as the best heat-conducting carrier fluids. Many of their applications comprise electric devices coolant, magnetic resonance imaging, and coolant of auto engines. The mixing of tiny particles in the pure fluid was first familiarized by Choi and Eastman [1] to expand the thermal performance of pure fluids. Acharya *et al.* [2] deliberated the effect of hydrothermal variations on radiative nanofluid flow subject to the impact of nanolayer as well as the diameter of nanoparticles and has established that with the use of nanoparticles, there is an enhancement of 84.61% in thermal performance of the fluid. Reddy *et al.* [3] numerical modeled the EMHD radiative transportation of Ti6Al4V-AA7075/H_2O nanofluids over a Riga surface. Shah *et al.* [4] used nanoparticles of gold in blood fluid flow between two surfaces with the influence of radiations and determined that with an upsurge in radiative factor and volume fraction, the heat flow progressed. Similarly, the thermal effectiveness of pure fluid can be heightened further by using two nanoparticles of different types and is termed a hybrid nanofluid. Chu *et al.* [5] described the hybrid nanofluid flow amid plates with the influence of particle shape and have established a good agreement with published results. Elsebaee *et al.* [6] modeled and simulated numerically the thermal transportation of silica-alumina hybrid nanoparticles past a slender surface. Khan *et al.* [7] studied the fluid flow with hybrid nanoparticles past a thermally heated needle subject to chemically reactive and bio-convective effects. Bharathi *et al.* [8] explored the thermally radiative flow of tangent hyperbolic trihybrid nanofluid flow across Darcy's porous surface. Alsaedi *et al.* [9] discussed hybrid MHD nanofluid flow amid two co-axial surfaces and deduced that there has been decay in temperature characteristics with higher values of copper volume fraction while Nusselt number has augmented in this process as depicted in their results during an investigation. Some recent studies may be found in the literature [10–15].

The fluids that are conducted electrically are counted as magneto-hydrodynamics (MHD) fluids. The flow of such fluid is fundamental in a wide range of industrial applications, like MHD generators, *etc*. Jayavel *et al.* [16] inspected the heat transference and irreversibility analysis through MHD Darcy–Forchheimer flow of hybrid nanoliquid over a wedge and cone. Kodi and Mopuri [17] examined MHD fluid flow over a vertical permeable and inclined surface using the impact of chemical reactions and heat absorption. Vishalakshi *et al.* [18] explored MHD fluid flow with mass transportation and slip conditions upon a stretching/shrinking surface and have verified that velocity and energy transition rise with the radiations and viscoelastic factors effects. Islam *et al.* [19] discussed the effects of Hall current on MHD fluid flow between two surfaces and deduced that augmentation in magnetic factor upsurge linear velocity and thermal characteristics while declining the rotational profiles of velocity. Sharma *et al.* [20] scrutinized MHD convective fluid flow past a rotating stretchable disk and highlighted that magnetic field strength was responsible for growth in Nusselt number. Raizah *et al.* [21] tested MHD fluid flow past a circular cylinder with the impact of dissipative energy and thermal radiations. Rehman *et al.* [22] conducted comparative work on thermal transportation for MHD fluid flow subject to thermal radiations past a plane as well as a cylindrical region and have proved that the thermal regime has more strength in the case of the cylindrical surface. Several researchers have recently reported on MHD fluid flow [23–26].

The fluid flow mechanisms through the porous surface in many problems are vibrant in science and industry, specifically in the petroleum industry. The thermal transportation phenomenon through a porous medium is practiced in many areas of science like geophysics and ceramic engineering, *etc*. Algehyne *et al.* [27] studied thermal transportation performance for fluid flow in a vertical porous sheet and determined that velocity characteristics have reduced both for nanoparticles and hybrid nanoparticles in the case of higher values of Darcy's and Forchheimer numbers. Qureshi *et al.* [28] examined mathematically the influence of nanofluid flow through a porous sheet by injecting SWCNTs and deduced that the effects of the thickness of the nano-layer were quite significant in the case of Nusselt number growth. Duguma *et al.* [29] inspected the stability analysis and dual solutions of Cu–H_2O–Casson nanoliquid flow past a stretching and shrinking slippery porous surface. Kumar *et al.* [30] deliberated numerically the heat transfer and Williamson fluid flow across a porous enlarging cylinder with the influence of heat generation and Joule heating. Khan *et al.* [31] inspected radiative MHD fluid flow subject to a non-uniform source of heat, rotating frame, and impacts of the Darcy-Forchheimer model. Shamshuddin *et al.* [32] studied a mathematical model for chemically reactive MHD nanofluid flow on a porous surface with the influence of Buongiorno's model

and concluded that the Sherwood number has elevated with greater values of reaction factor. Alqahtani *et al.* [33] explored numerically the thermal transportation for radiative MHD Jeffery fluid flow in a permeable stretched surface. Duguma *et al.* [34] discussed the stagnation point flow of TiO_2–$CoFe_2O_4/H_2O$–Casson nanofluid over a slippery stretching cylindrical porous medium. Furthermore, some remarkable results may be found in previous studies [35–39].

Various mathematical models are applied to examine the behavior of fluids and flow properties. The famous model of Buongiorno's [40] has also been established to focus on seven different procedures and processes inside fluid flow. In these seven effects, thermophoresis and Brownian motion effects are more substantial. Mishra and Upreti [41] conducted a comparative analysis of the fluid flow across a curved surface by using the impact of Buongiorno's model and realized that fluid motion has weakened and heat flow has expanded for progression in the Brownian factor. Elattar *et al.* [42] numerically analyzed the flow of nanofluid film subject to heat production with Buongiorno's model. Upreti *et al.* [43] studied the effect of homogeneous–heterogeneous reactions on the MHD Sisko nanofluid flow across an elongating surface with the convective conditions and Buongiorno's model. Safdar *et al.* [44] examined EMHD nanoparticle fluid flow on a stretched surface with the impact of activated energy, buoyancy force, microorganisms, and Buongiorno's model and have deduced that with augmentation in mixed convection factor, there has been a growth in Nusselt number while velocity field degenerated with incrimination in viscosity factor. Puneeth *et al.* [45] implemented a modified Buongiorno's model for the examination of chemically reactive trihybrid nanofluid flow using bioactive mixers. Rasool *et al.* [46] investigated MHD Maxwell nanoliquid flow past an extending surface and proved that the porosity factor supported the drag force/skin friction. Hussain *et al.* [47] debated Maxwell nanofluid flow in a solar collector by using modified Buongiorno's model and explored that temperature field upsurges with growth in radiation factor and has declined with upsurge in Schmidt number and reactive factor.

In different fields, various chemical reactions are needed to analyze different flow systems. Some of these reactions are associated with catalysts. These reactions can be seen in many applications and processes at the industrial level. Shoaib *et al.* [48] discussed the production of entropy for fluid flow with quadratic order chemical reaction and highlighted that skin friction has augmented with growth in radiation factor. Bilal *et al.* [49] analyzed computationally a time-based MHD trihybrid nanofluid using the impacts of chemically reactive activation energy and deduced that the mass curve intensified with the upsurge in Lewis number, reaction, and activation factors. Ahmed *et al.* [50] explored numerically the hydrothermal fully developed hybrid nanoliquid flow across an annular sector. Goud *et al.* [51] discussed computationally the significance of chemically reactive effects on MHD fluid flow past a Riga plate and have proved that with growth in Hartman number, there is a growth in velocity characteristics at free stream. Sajid *et al.* [52] discussed the impacts of MHD on the fluid flow with the consequence of chemical reaction and heat source/sink. Zeeshan *et al.* [53] inspected the non-Newtonian fluid flow across a horizontal surface. Shah *et al.* [54] examined the bioconvective impact on nanofluid flow subject to chemical reactions and microorganisms past an extending surface. Wang *et al.* [55] discussed the production of entropy optimization with Darcy–Forchheimer model-based fluid flow with the effect of a chemical reaction and noticed that velocity profiles have weakened with slip and porosity factors.

The interaction of nanoparticles (NPs) with carrier red blood cells (RBCs) is profoundly altered by attachment to the surface of these cells, resulting in a deceleration of their clearance from the bloodstream, and facilitation of their transfer from the surface of these cells to the vascular cells. Many drug delivery purposes benefit from these changes in NP pharmacokinetics imposed by carrier RBCs. Using blood as a nanoparticle, many researchers have studied different types of mathematical problems for different types of physical surfaces [56–60]. The significance of blood-based Casson hybrid nanofluid flow comprising of gold and ferrous oxide nanoparticles contains many healthcare and biomedical engineering. Those fluids which contain metallic nanoparticles like Au and Fe_3O_4 nanoparticles can significantly enhance the thermal conductivity of the base fluid. The present investigation deals with the blood-based Casson hybrid nanofluid flow comprising gold and ferrous oxide nanoparticles over a stretching surface using porous media. According to the authors' knowledge, this topic has not yet been presented numerically. Additionally, some external forces like thermal radiation and Joule heating are taken into consideration. The sheet surface is kept with a hot working fluid (blood). Also, a non-Newtonian Casson model is adopted to hold the non-Newtonian fluid properties. Thus, the following research questions have to be answered:

1) In which case, *i.e.*, blood-based nanofluid or hybrid nanofluid, do the embedding factors have dominant impacts on the flow profiles?
2) What is the role of angle of inclination in terms of velocity and temperature of the blood-based nanofluid or hybrid nanofluid?
3) How do the skin friction and local Nusselt number increase/decrease *via* differential entrenching factors?

In order to answer the above research questions, we have presented this article section-wise. Section 2 shows the problem formulation. Section 3 demonstrates the numerical analysis of the present model. Section 4 displays the code validation of the present analysis. Section 5 displays the results and discussion while Section 6 presents the concluding remarks.

2 Formulation of problem

Assume the two-dimensional flow of a Casson hybrid nanofluid past as a stretching surface using porous media. Gold and ferrous oxide are taken as two different nanoparticles and dispersed in blood which is used as base fluid. The sheet is stretched along x-axis with velocity $u_w(x) = ax$ with $a > 0$. The strength of the magnetic field is B_0 that is employed perpendicular (along y-axis) to the nanofluid flow as shown in Figure 1. The surface temperature is denoted by T_w. Also, the reference temperature is denoted by T_f such that $T_f > T_w$. The ambient temperature is denoted by T_∞. Additionally, the Joule heating, heat source, exponential heat source and thermal radiation effects are considered in this work.

The rheological equation of a Casson fluid flow is defined as:

$$\tau_{ij} = \begin{cases} 2\left(\mu_B + \dfrac{P_y}{\sqrt{2\pi}}\right)e_{ij}, & \pi > \pi_c \\ 2\left(\mu_B + \dfrac{P_y}{\sqrt{2\pi_c}}\right)e_{ij}, & \pi < \pi_c, \end{cases} \tag{1}$$

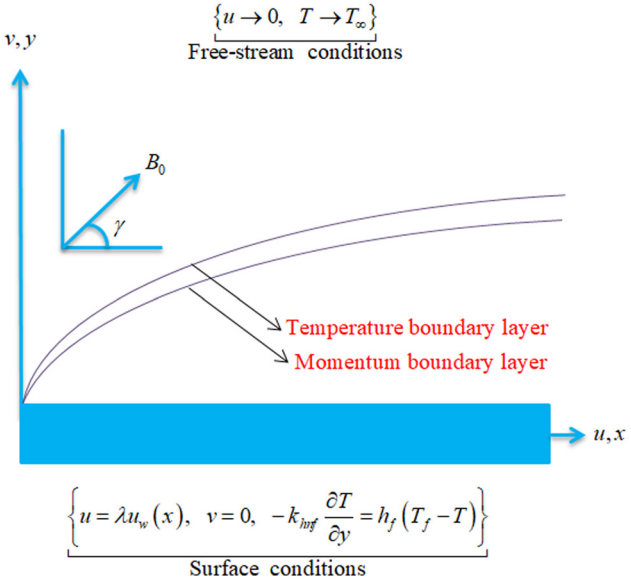

Figure 1: Geometrical view of the flow problem.

where μ_B shows the plastic dynamic viscosity, P_y shows the yield stress, $\pi = e_{ij}e_{ij}$ where e_{ij} is the (i, j)th deformation rate component and π_c is the critical value of this product.

The governing equations in vector form can be written as:

$$\nabla \cdot \boldsymbol{V} = 0, \tag{2}$$

$$\frac{\partial \boldsymbol{V}}{\partial t} + (\boldsymbol{V}\cdot\nabla)\boldsymbol{V} = -\frac{1}{\rho_{hnf}}\nabla P + \frac{\mu_{hnf}}{\rho_{hnf}}\left(1 + \frac{1}{\beta}\right)\nabla^2\boldsymbol{V} - \frac{\sigma_{hnf}}{\rho_{hnf}}(\boldsymbol{J}\times\boldsymbol{B}) - \frac{\mu_{hnf}}{\rho_{hnf}K_p}\left(1 + \frac{1}{\beta}\right)\boldsymbol{V}, \tag{3}$$

$$\left\{\begin{aligned} &\frac{\partial T}{\partial t} + (\boldsymbol{V}\cdot\nabla)T = -\frac{\nabla\cdot\boldsymbol{q}}{(\rho C_p)_{hnf}} + \frac{Q_t(T - T_\infty)}{(\rho C_p)_{hnf}} \\ &\qquad + \frac{\boldsymbol{J}^2}{(\rho C_p)_{hnf}\sigma_{hnf}} + \frac{Q_e(T_f - T_\infty)}{(\rho C_p)_{hnf}}\exp\left(-n\sqrt{\frac{a}{\nu_f}}y\right) \\ &\text{where}\left\{\boldsymbol{q} = \boldsymbol{q}_R + \boldsymbol{q}_F,\ \boldsymbol{q}_F = -k_{hnf}\nabla T,\ \boldsymbol{q}_R = -\frac{4\sigma^*}{3k^*}\nabla T^4\right\} \end{aligned}\right\}. \tag{4}$$

Thus, the leading equations in partial differential form can be described as [61–64]:

$$\frac{\partial u}{\partial x} + \frac{\partial v}{\partial y} = 0, \tag{5}$$

$$u\frac{\partial u}{\partial x} + v\frac{\partial u}{\partial y} = \left(1 + \frac{1}{\beta}\right)\frac{\mu_{hnf}}{\rho_{hnf}}\frac{\partial^2 u}{\partial y^2} - \frac{\mu_{hnf}}{\rho_{hnf}}\left(1 + \frac{1}{\beta}\right)\frac{u}{K_p} - \frac{\sigma_{hnf}}{\rho_{hnf}}B_0^2 u\sin^2\gamma, \tag{6}$$

$$u\frac{\partial T}{\partial x} + v\frac{\partial T}{\partial y} = \frac{1}{(\rho C_p)_{hnf}}\left(k_{hnf} + \frac{16\sigma^* T_\infty^3}{3k^*}\right)\frac{\partial^2 T}{\partial y^2} + \frac{\sigma_{hnf}}{(\rho C_p)_{hnf}}B_0^2 u^2\sin^2\gamma + \frac{1}{(\rho C_p)_{hnf}}Q_t(T - T_\infty) + \frac{1}{(\rho C_p)_{hnf}}Q_e(T_f - T_\infty)\exp\left(-n\sqrt{\frac{a}{\nu_f}}y\right), \tag{7}$$

In the above equations, u, v are the velocity components, x, y are the coordinate axes, μ is the dynamic viscosity, ρ is the density, K_p is the permeability of the porous medium, σ is the electrical conductivity, γ is the angle of inclination, C_p is the specific heat, k is the thermal conductivity, σ^* is the Stefan-Boltzmann constant, k^* is the mean absorption coefficient, Q_t is the constant heat source coefficient, and Q_e is the exponential heat source coefficient.

The boundary conditions are [61–64]:

$$\left.\begin{aligned} &u = u_{\mathrm{w}}(x)\lambda, \quad v = 0, \quad -k_{\mathrm{hnf}}\frac{\partial T}{\partial y} = h_{\mathrm{f}}(T_{\mathrm{f}} - T),\\ &\text{at} \quad y = 0,\\ &\quad u \to 0, \quad T \to T_{\infty} \quad \text{as} \quad y \to \infty, \end{aligned}\right\} \tag{8}$$

where $\lambda > 0$ shows the stretching case of the sheet, and $\lambda < 0$ shows shrinking case of the sheet.

The effective characteristics of the nanofluid and hybrid nanofluid are defined as [65]:

$$\mu_{\mathrm{nf}} = \frac{\mu_{\mathrm{f}}}{(1-\varphi_1)^{2.5}}, \quad \mu_{\mathrm{hnf}} = \frac{\mu_{\mathrm{f}}}{(1-\varphi_1)^{2.5}(1-\varphi_2)^{2.5}}, \tag{9}$$

$$\begin{aligned} &\rho_{\mathrm{nf}} = \rho_{\mathrm{f}}(1-\varphi_1) + \varphi_1\rho_{N_1}, \quad \rho_{\mathrm{hnf}} = (1-\varphi_2)\\ &\{\rho_{\mathrm{f}}(1-\varphi_1) + \varphi_1\rho_{N_1}\} + \varphi_2\rho_{N_2}, \end{aligned} \tag{10}$$

$$\begin{aligned} (\rho C_p)_{\mathrm{nf}} &= (\rho C_{\mathrm{p}})_{\mathrm{f}}(1-\varphi_1) + (\rho C_{\mathrm{p}})_{N_1}\varphi_1,\\ (\rho C_{\mathrm{p}})_{\mathrm{hnf}} &= \{(\rho C_{\mathrm{p}})_{\mathrm{f}}(1-\varphi_1) + \varphi_1(\rho C_{\mathrm{p}})_{N_1}\}(1-\varphi_2)\\ &\quad + (\rho C_{\mathrm{p}})_{N_2}\varphi_2. \end{aligned} \tag{11}$$

$$\begin{aligned} \frac{k_{\mathrm{nf}}}{k_{\mathrm{f}}} &= \frac{k_{N_1} + 2k_{\mathrm{f}} - 2\varphi_1(k_{\mathrm{f}} - k_{N_1})}{k_{N_1} + 2k_{\mathrm{f}} + \varphi_1(k_{\mathrm{f}} - k_{N_1})},\\ \frac{k_{\mathrm{hnf}}}{k_{\mathrm{nf}}} &= \frac{k_{N_2} + 2k_{\mathrm{f}} - 2\varphi_2(k_{\mathrm{f}} - k_{N_2})}{k_{N_2} + 2k_{\mathrm{f}} + \varphi_2(k_{\mathrm{f}} - k_{N_2})}. \end{aligned} \tag{12}$$

$$\begin{aligned} \frac{\sigma_{\mathrm{nf}}}{\sigma_{\mathrm{f}}} &= \frac{\sigma_{N_1} + 2\sigma_{\mathrm{f}} - 2(\sigma_{\mathrm{f}} - \sigma_{N_1})\varphi_1}{\sigma_{N_1} + 2\sigma_{\mathrm{f}} + (\sigma_{\mathrm{f}} - \sigma_{N_1})\varphi_1},\\ \frac{\sigma_{\mathrm{hnf}}}{\sigma_{\mathrm{nf}}} &= \frac{\sigma_{N_2} + 2\sigma_{\mathrm{f}} - 2(\sigma_{\mathrm{f}} - \sigma_{N_2})\varphi_2}{\sigma_{N_2} + 2\sigma_{\mathrm{f}} + (\sigma_{\mathrm{f}} - \sigma_{N_2})\varphi_2}. \end{aligned} \tag{13}$$

Here, N_1 and N_2 represent the first and second nanoparticles with φ_1 and φ_2 as their volume fractions, respectively. Thermophysical features of the nanoparticles and base fluid are defined in Table 1.

To reduce the above system of Eqs. (5)–(7), the following similarity variables are described as [64]:

$$\begin{aligned} &u = axf'(\eta), \quad v = -\sqrt{\nu_{\mathrm{f}}a}f(\eta),\\ &T = T_{\infty} + (T_{\mathrm{f}} - T_{\infty})\theta(\eta), \quad \eta = y\sqrt{\frac{a}{\nu_{\mathrm{f}}}}. \end{aligned} \tag{14}$$

So, Eq. (5) is satisfied, and the remaining equations are as follows:

Table 1: Thermophysical features of pure fluid and nanoparticles [65]

Physical property	Blood	Fe_3O_4	Au
ρ	1,063	5,180	19,300
C_{p}	3,750	670	129
k	0.429	9.7	318
σ	4.3×10^{-5}	0.74×10^{6}	4.1×10^{6}

$$\begin{aligned} &\frac{\xi_1}{\xi_2}\left(1 + \frac{1}{\beta}\right)f'''(\eta) - f'^2(\eta) + f''(\eta)f(\eta) - \frac{\xi_3}{\xi_2}M\sin^2\gamma f'(\eta)\\ &\quad + \frac{\xi_1}{\xi_2}K\left(1 + \frac{1}{\beta}\right)f'(\eta) = 0, \end{aligned} \tag{15}$$

$$\begin{aligned} &\frac{1}{\xi_5}(\xi_4 + \mathrm{Rd})\theta''(\eta) + \mathrm{Pr}\, f(\eta)\theta'(\eta)\\ &\quad + \frac{\mathrm{Pr}}{\xi_5}(\xi_3 M\mathrm{Ec}\sin^2\gamma f'^2(\eta) + Q_{\mathrm{E}}\exp(-n\eta) + Q_{\mathrm{I}}\theta(\eta))\\ &= 0. \end{aligned} \tag{16}$$

Related conditions are as follows:

$$\left\{\begin{aligned} &f(0) = 0, \quad f'(0) = \lambda, \quad f'(\infty) \to 0\\ &\frac{k_{\mathrm{hnf}}}{k_{\mathrm{f}}}\theta'(0) = -B_{\mathrm{T}}(1 - \theta(0)), \quad \theta(\infty) \to 0 \end{aligned}\right\}. \tag{17}$$

In the above equations, Pr is the Prandtl number, M is the magnetic factor, Rd is the radiative factor, Ec is the Eckert number, Q_{E} is the space-dependent heat source factor, Q_{I} shows the space-dependent heat source, and B_{T} indicates the thermal Biot number. All these parameters are defined as [61–64]:

$$\left\{\begin{aligned} &\xi_1 = \frac{\mu_{\mathrm{hnf}}}{\mu_{\mathrm{f}}}, \quad \xi_2 = \frac{\rho_{\mathrm{hnf}}}{\rho_{\mathrm{f}}}, \quad \xi_3 = \frac{\sigma_{\mathrm{hnf}}}{\sigma_{\mathrm{f}}}, \quad \xi_4 = \frac{k_{\mathrm{hnf}}}{k_{\mathrm{f}}},\\ &\xi_5 = \frac{(\rho C_{\mathrm{p}})_{\mathrm{hnf}}}{(\rho C_{\mathrm{p}})_{\mathrm{f}}}, \quad M = \frac{\sigma_{\mathrm{f}}B_0^2}{a\rho_{\mathrm{f}}}, \quad \mathrm{Ec} = \frac{u_{\mathrm{w}}^2}{(C_{\mathrm{p}})_{\mathrm{f}}(T_{\mathrm{f}} - T_{\infty})},\\ &B_{\mathrm{T}} = \frac{h_{\mathrm{f}}}{k_{\mathrm{f}}}\sqrt{\frac{\nu_{\mathrm{f}}}{a}}, \quad \mathrm{Pr} = \frac{\nu_{\mathrm{f}}(\rho C_{\mathrm{p}})_{\mathrm{f}}}{k_{\mathrm{f}}}, \quad K = \frac{\mu_{\mathrm{f}}}{a\rho_{\mathrm{f}}K_{\mathrm{p}}},\\ &\mathrm{Rd} = \frac{16\sigma^*T_{\infty}^3}{3k^*k_{\mathrm{f}}}, \quad Q_{\mathrm{E}} = \frac{Q_t}{a(\rho C_{\mathrm{p}})_{\mathrm{f}}}, \quad Q_{\mathrm{I}} = \frac{Q_{\mathrm{e}}}{a(\rho C_{\mathrm{p}})_{\mathrm{f}}}. \end{aligned}\right\} \tag{18}$$

The quantities of importance like skin friction (C_{fx}) and local Nusselt number (Nu_x) are described as:

$$C_{\mathrm{fx}} = \frac{\tau_{\mathrm{w}}}{\rho_{\mathrm{f}}(u_{\mathrm{w}}(x))^2}, \quad \mathrm{Nu}_x = \frac{xq_{\mathrm{w}}}{k_{\mathrm{f}}(T_{\mathrm{f}} - T_{\infty})}, \tag{19}$$

where

$$\begin{aligned} \tau_{\mathrm{w}} &= \mu_{\mathrm{hnf}}\frac{\partial u}{\partial y}\bigg|_{y=0},\\ q_{\mathrm{w}} &= -k_{\mathrm{hnf}}\left(\frac{\partial T}{\partial y}\bigg|_{y=0} - \frac{16\sigma^*}{3k^*}\frac{\partial T^4}{\partial y}\bigg|_{y=0}\right). \end{aligned} \tag{20}$$

Thus, Eq. (20) reduces as follows:

$$\sqrt{\mathrm{Re}_x}C_{\mathrm{fx}} = \xi_1 f''(0), \quad \frac{\mathrm{Nu}_x}{\sqrt{\mathrm{Re}_x}} = -(\xi_4 + \mathrm{Rd})\theta'(0), \tag{21}$$

where $\mathrm{Re}_x = \frac{ax^2}{\nu_{\mathrm{f}}}$ is the local Reynolds number.

3 Numerical solution

To investigate the numerical solution of the proposed model presented in Eqs (15) and (16) with conditions at boundaries given in Eq. (17), the Matlab built-in package (bvp4c) is adopted [66–70]. To perform the bvp4c technique, first, we have to reduce the model equations into first-order differential equations. Thus, we have assumed the following relations:

$$\left.\begin{array}{l} f(\xi) = \varkappa(1), \quad f'(\xi) = \varkappa(2), \quad f''(\xi) = \varkappa(3), \\ f'''(\xi) = \varkappa'(3), \\ \theta(\xi) = \varkappa(4), \quad \theta'(\xi) = \varkappa(5), \quad \theta''(\xi) = \varkappa'(5). \end{array}\right\} \tag{22}$$

Then the leading equation can be written as: with boundary conditions:

$$\varkappa'(3) = -\frac{\varkappa(1)\varkappa(3) - (\varkappa(2))^2 - \frac{\xi_3}{\xi_2}M\sin^2\gamma\varkappa(2) + \frac{\xi_1}{\xi_2}\left(1+\frac{1}{\beta}\right)K\varkappa(2)}{\frac{\xi_1}{\xi_2}\left(1+\frac{1}{\beta}\right)}, \tag{23}$$

$$\varkappa'(5) = -\frac{\mathrm{Pr}\varkappa(1)\varkappa(5) + \frac{\mathrm{Pr}}{\xi_5}(\xi_3 M\mathrm{Ec}\sin^2\gamma(\varkappa(2))^2 + Q_{\mathrm{E}}\exp(-n\eta) + Q_I\varkappa(4))}{\frac{1}{\xi_5}(\xi_4+\mathrm{Rd})}, \tag{24}$$

$$\left.\begin{array}{l} \varkappa_{\mathrm{a}}(1) - 0, \quad \varkappa_{\mathrm{a}}(2) - \lambda, \quad \varkappa_{\mathrm{b}}(2) - 0, \\ \frac{k_{\mathrm{hnf}}}{k_{\mathrm{f}}}\varkappa_{\mathrm{a}}(5) + B_{\mathrm{T}}(1 - \varkappa_{\mathrm{a}}(4)), \quad \varkappa_{\mathrm{b}}(4) - 0 \end{array}\right\}. \tag{25}$$

The quantities of interest can be written as:

$$\sqrt{\mathrm{Re}_x}C_{\mathrm{fx}} = \frac{\mu_{\mathrm{hnf}}}{\mu_{\mathrm{f}}}\varkappa_{\mathrm{a}}(3), \quad \frac{\mathrm{Nu}_x}{\sqrt{\mathrm{Re}_x}} = -(\xi_4+\mathrm{Rd})\varkappa_a(5). \tag{26}$$

4 Code validation

Validation of the obtained results of $-\theta'(0)$ from the previous and present analysis is shown in Table 2. This table shows the comparison of present and previously published results which can confirm and validate the code of this problem. Additionally, one can say that the designed mathematical model is valid and can be extended for further analysis.

Table 2: Validation of $\theta'(0)$ for different values of Pr while all other factors are zero

Pr	$\theta'(0)$	
	Hamad [71]	**Present results**
0.07	0.06556	0.0655797
0.2	0.16909	0.1690994
0.7	0.45391	0.4539206
2.0	0.91136	0.9113705
7.0	1.89540	1.8954015

5 Results and discussion

We have analyzed the blood-based Casson hybrid nanofluid flow composed of Au and Fe_3O_4 NPs over a convectively heated permeable surface. The default values of embedded factors are taken as Pr = 21, M = 1.0, K = 0.5, Rd = 0.5, Ec = 0.1, $Q_{\mathrm{E}} = Q_{\mathrm{I}}$ = 0.3 and B_{T} = 0.5. The significances of flow constraints against the velocity and energy profiles are displayed in the form of figures as well as tables. Figure 1 exhibits the physical representation of the hybrid nanoliquid flow. Figures 2 and 3 elaborate the effect of magnetic factor (M) on $f'(\xi)$ and $\theta(\xi)$ for both cases hybrid (Au–Fe_3O_3/blood) and nanofluid (Au/blood). Physically, the magnetic effect generates the resistive force which contests to the motion of fluid, and results in lowering the velocity curve as shown in Figure 2. That resistive effect is known as Lorentz force, stated as the combination of the electric and magnetic force due to electromagnetic flux on a point charge. On the other side, the energy profile rises for flourishing impact of (M). Actually, the free particles move over the sheet surface and some of them crash due to friction force, these collisions amongst particles of fluid produce heat and "resistance" to the fluid motion. Figures 4 and 5 show the impression of inclination angle (γ) on $f'(\xi)$ and $\theta(\xi)$ for both cases hybrid (Au–Fe_3O_4/blood) and nanofluid (Au/blood). It can be detected that both the temperature and velocity curve drop for upsurge in angle of inclination. Physically, the increasing angle of inclination boosts the Lorentz force which reduces the velocity profile. On the other hand, the greater angle of inclination reduces the thermal boundary layer thickness which results reduction in the temperature profile. Figures 6 and 7 show the

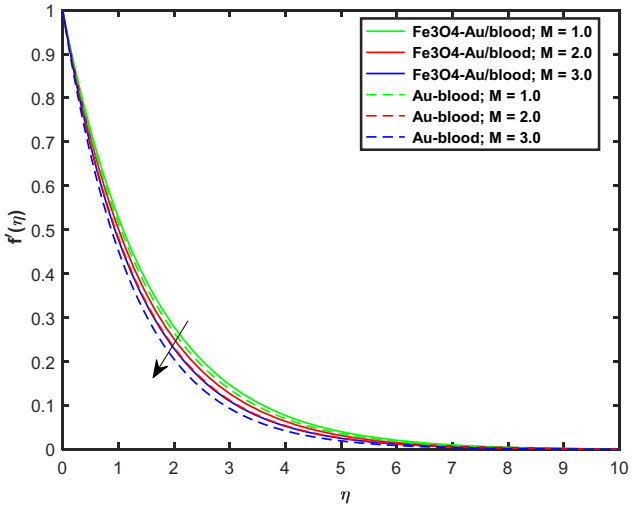

Figure 2: Variation in $f'(\xi)$ *via* M.

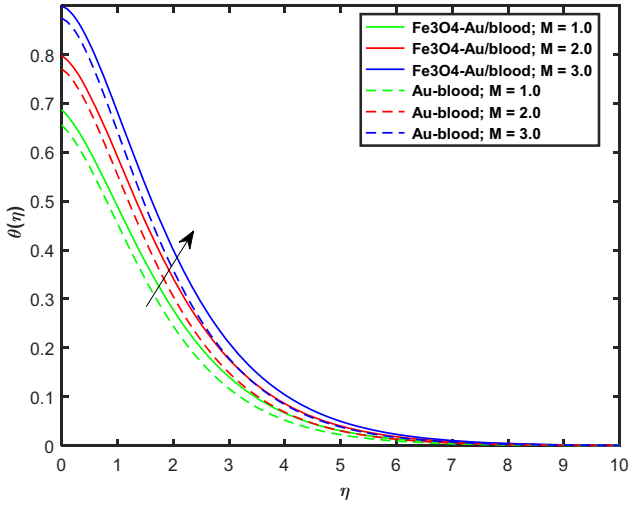

Figure 3: Variation in $\theta(\xi)$ *via* M.

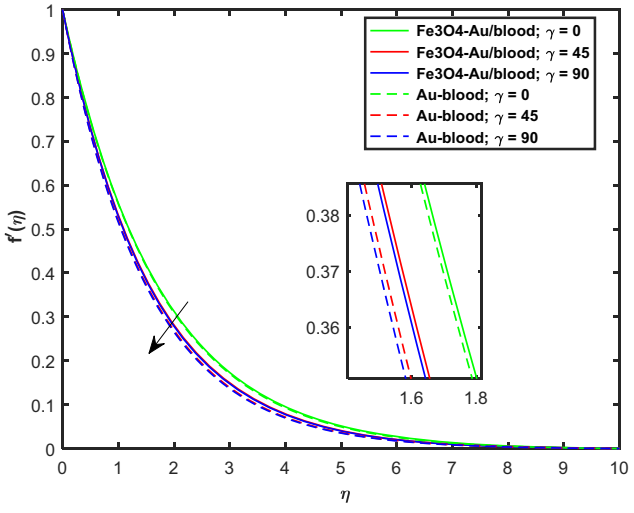

Figure 4: Variation in $f'(\xi)$ *via* γ.

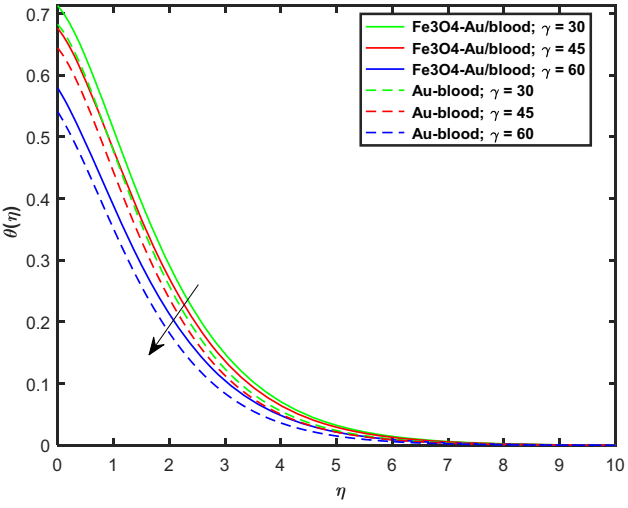

Figure 5: Variation in $\theta(\xi)$ *via* γ.

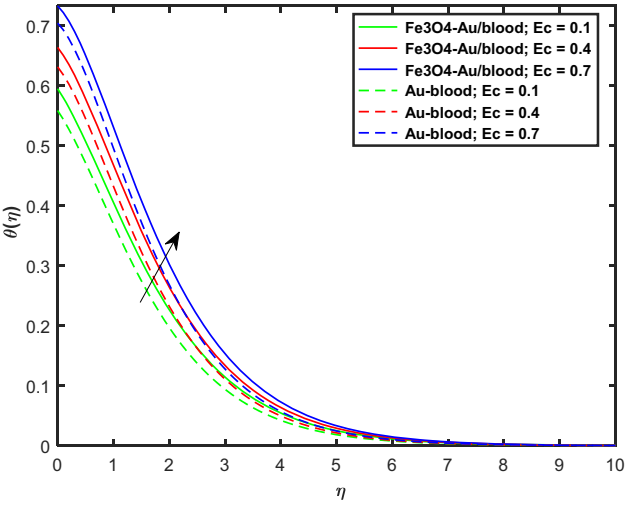

Figure 6: Variation in $\theta(\xi)$ *via* Ec.

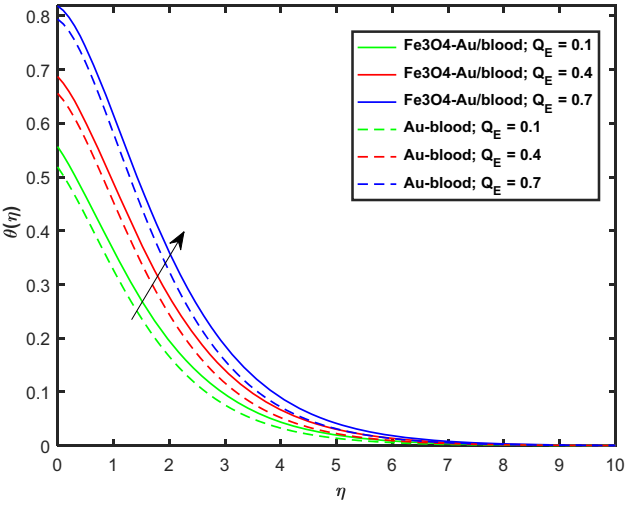

Figure 7: Variation in $\theta(\xi)$ *via* Q_{E}.

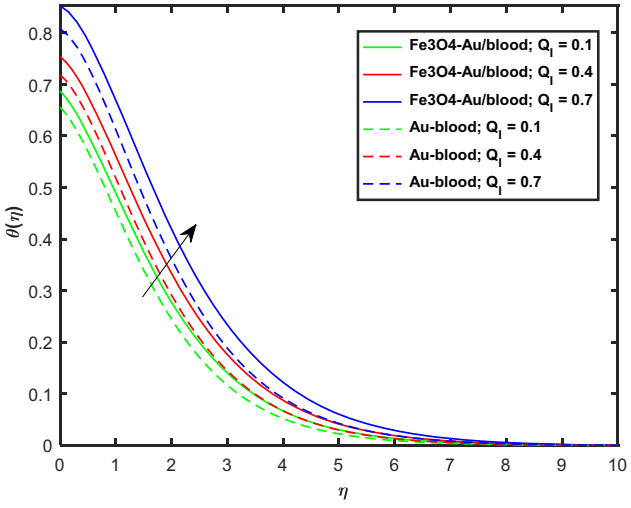

Figure 8: Variation in $\theta(\xi)$ *via* Q_{I}.

impression of Eckert number (Ec) and heat source factor (space-dependent) Q_{E} on $\theta(\xi)$, respectively. Physically, the Eckert number is the relation between advection transpport and heat dissipation and used to describe the energy transport dissipation. So, the inverse relation of heat dissipation potentional with the Ec enhances the fluid temoperature as displayed in Figure 6. Figure 7 demonstrates that the influence of heat source term Q_{E} on the energy curve $\theta(\xi)$. The higher Q_{E} augments $\theta(\xi)$. Physically, the specific heat capacity of base fluid deteriorates with the effect of Q_{E} which results in the advancement of the energy curve. Figure 8 demonstrates that the influence of heat source term Q_{I} on the energy curve $\theta(\xi)$. The higher Q_{I} augments $\theta(\xi)$. Physically, the specific heat capacity of base fluid deteriorates with the effect of Q_{I} which results in the advancement of the energy curve. Table 1 particularizes the experimental values used in the approximation of the model equations of nanoparticles Fe_3O_4 and Au, and blood. Tables 3 and 4 reveal numerically the impression on $\sqrt{\mathrm{Re}_x}C_{\mathrm{fx}}$ and $\frac{\mathrm{Nu}_x}{\sqrt{\mathrm{Re}_x}}$. From Table 3, it can be noticed that the variability of the magnetic term gradually enhances the skin friction. Because due to resistive effect produced by magnetic field enhances the drag force $\sqrt{\mathrm{Re}_x}C_{\mathrm{fx}}$. Table 4 shows the statistical outcomes for both the cases nanofluid (Au/blood) and hybrid nanoliquid (Fe_3O_4-Au/blood) *versus* the variation of distinct physical constraints. From Table 4, it can be noticed that the energy transmission rate, in case of (Fe_3O_4-Au/blood) hybrid nanoliquid is much hgher as compared to the nanofluid case.

Table 3: Variation in skin friction *via* M

M	$\sqrt{\mathrm{Re}_x}C_{\mathrm{fx}}$	
	Fe_3O_4–Au/blood	Au–blood
0.1	1.1157	1.1065
0.2	1.1165	1.1069
0.3	1.1173	1.1074

Table 4: Variation in Nusselt number *via* M, Rd, Q_{E}, and Ec

M	Rd	Q_{E}	Ec	$\frac{\mathrm{Nu}_x}{\sqrt{\mathrm{Re}_x}}$	
				Fe_3O_4–Au/blood	Au–blood
0.1	0.5	0.1	0.1	0.3052	0.2969
0.2				0.3038	0.2939
0.3				0.3024	0.2905
	1.0			0.4094	0.4157
	1.1			0.4303	0.4274
	1.2			0.4511	0.4373
		0.1		0.5112	0.4964
		0.2		0.4467	0.4075
		0.3		0.3783	0.2989
			1.0	0.3035	0.2896
			2.0	0.3007	0.2846
			3.0	0.2979	0.2789

6 Conclusion

In this work, hybrid nanofluid flow consisting of Fe_3O_4 and Au NPs over a convectively heated permeable sheet has been investigated. The flow of fluid is formulated using the system of partial differential equations (PDEs). The modeled equations of PDEs are transformed into the set of ordinary differential equations (ODEs) by using the similarity substitution. The Matlab built-in package (bvp4c) is employed to solve the transform nonlinear set of ODEs. The main conclusions are as follows:

- By raising the angle of inclination, both the velocity and temperature profiles are reduced. Furthermore, the magnetic factor increases the temperature distribution while reduces the velocity distribution.
- Growth in Eckert number, thermal-dependent heat source and the space-dependent heat source factor accelerates the temperature profile.
- The energy transfer rate boosts with the consequence of the radiation factor, whereas drops with the impact of the Eckert number.
- The velocity and temperature distributions are very effective in the cases of hybrid nanofluid (Au–F_e3O_4/blood) when compared to nanofluid (Au/blood).
- The skin friction and rate of heat transfer are very effective in the cases of hybrid nanofluid (Au–Fe_3O_4/blood) when compared to nanofluid (Au/blood).

Funding information: The authors extend their appreciation to the Deanship of Scientific Research at King Khalid University, Abha, Saudi Arabia, for funding this work through the Research Group Project under Grant Number (RGP.2/505/44). This work was supported by the Deanship of Scientific Research, the Vice Presidency for Graduate Studies and Scientific Research, King Faisal University, Saudi Arabia (Grant No. 5580).

Author contributions: All authors have accepted responsibility for the entire content of this manuscript and approved its submission.

Conflict of interest: The authors state no conflict of interest.

Data availability statement: The datasets generated and/or analyzed during the current study are available from the corresponding author on reasonable request.

References

[1] Choi SU, Eastman JA. Enhancing thermal conductivity of fluids with nanoparticles. Argonne National Lab. (ANL), Argonne, IL (United States): 1995 Oct.

[2] Acharya N, Mabood F, Shahzad SA, Badruddin IA. Hydrothermal variations of radiative nanofluid flow by the influence of nanoparticles diameter and nanolayer. Int Commun Heat Mass Transf. 2022 Jan;130:105781.

[3] Reddy MG, Tripathi D, Bég OA, Tiwari AK. Numerical modelling of electromagnetohydrodynamic (EMHD) radiative transport of hybrid Ti6Al4V-AA7075/H_2O nanofluids from a riga plate sensor surface. In: Nanomaterials and Nanoliquids: Applications in Energy and Environment. Singapore: Springer Nature Singapore; 2023 Nov. p. 225–48.

[4] Shah Z, Khan A, Khan W, Alam MK, Islam S, Kumam P, et al. Micropolar gold blood nanofluid flow and radiative heat transfer between permeable channels. Comput Methods Prog Biomed. 2020 Apr;186:105197.

[5] Chu YM, Bashir S, Ramzan M, Malik MY. Model-based comparative study of magnetohydrodynamics unsteady hybrid nanofluid flow between two infinite parallel plates with particle shape effects. Math Methods Appl Sci. 2023 Jul;46(10):11568–82.

[6] Elsebaee FA, Bilal M, Mahmoud SR, Balubaid M, Shuaib M, Asamoah JK, et al. Motile micro-organism based trihybrid nanofluid flow with an application of magnetic effect across a slender stretching sheet: Numerical approach. AIP Adv. 2023 Mar;13(3).

[7] Khan A, Saeed A, Tassaddiq A, Gul T, Kumam P, Ali I, et al. Bioconvective and chemically reactive hybrid nanofluid flow upon a thin stirring needle with viscous dissipation. Sci Rep. 2021 Apr;11(1):8066.

[8] Barathi V, Prakash J, Tripathi D, Beg O, Sharma A, Sharma RK. Heat transfer in EMHD hyperbolic tangent ternary hybrid nanofluid flow over a Darcy-Forchheimer porous wedge surface: A numerical simulation. Springer; 2023.

[9] Alsaedi A, Muhammad K, Hayat T. Numerical study of MHD hybrid nanofluid flow between two coaxial cylinders. Alex Eng J. 2022 Nov;61(11):8355–62.

[10] Upreti H, Mishra SR, Pandey AK, Bartwal P. Shape factor analysis in stagnation point flow of Casson nanofluid over a stretching/shrinking sheet using Cattaneo–Christov model. Numer Heat Transf Part B: Fundam. 2023 Oct;1–7.

[11] Upreti H, Mishra SR, Kumar Pandey A, Joshi N, Joshi BP. Diversified role of fuzzified particle concentration on Casson gold-blood nanofluid flow through an elongating sheet for different shape nanoparticles. J Taibah Univ Sci. 2023 Dec;17(1):2254465.

[12] Sajid T, Gari AA, Jamshed W, Eid MR, Islam N, Irshad K, et al. Case study of autocatalysis reactions on tetra hybrid binary nanofluid flow via Riga wedge: Biofuel thermal application. Case Stud Therm Eng. 2023 Jul;47:103058.

[13] Prakash J, Tripathi D, Bég OA. Computation of EMHD ternary hybrid non-Newtonian nanofluid over a wedge embedded in a Darcy-Forchheimer porous medium with zeta potential and wall suction/injection effects. Int J Ambient Energy. 2023;44(1):2155–69.

[14] Alharbi KA, Ahmed AE, Sidi MO, Ahammad NA, Mohamed A, El-Shorbagy MA, et al. Computational valuation of darcy ternary-hybrid nanofluid flow across an extending cylinder with induction effects. Micromachines. 2022;13:588.

[15] Tadesse FB, Makinde OD, Enyadene LG. Hydromagnetic stagnation point flow of a magnetite ferrofluid past a convectively heated permeable stretching/shrinking sheet in a Darcy–Forchheimer porous medium. Sādhanā. 2021 Sep;46(3):115.

[16] Jayavel P, Upreti H, Tripathi D, Pandey AK. Irreversibility and heat transfer analysis in MHD Darcy-Forchheimer flow of Casson hybrid nanofluid flow through cone and wedge. Numer Heat Transf Part A: Appl. 2023 Sep;1–27.

[17] Kodi R, Mopuri O. Unsteady MHD oscillatory Casson fluid flow past an inclined vertical porous plate in the presence of chemical reaction with heat absorption and Soret effects. Heat Transf. 2022 Jan;51(1):733–52.

[18] Vishalakshi AB, Mahabaleshwar US, Sarris IE. An MHD fluid flow over a porous stretching/shrinking sheet with slips and mass transpiration. Micromachines. 2022 Jan;13(1):116.

[19] Islam S, Khan A, Deebani W, Bonyah E, Alreshidi NA, Shah Z. Influences of Hall current and radiation on MHD micropolar non-Newtonian hybrid nanofluid flow between two surfaces. AIP Adv. 2020 May;10(5).

[20] Sharma K, Kumar S, Narwal A, Mebarek-Oudina F, Animasaun IL. Convective MHD fluid flow over stretchable rotating disks with dufour and soret effects. Int J Appl Comput Math. 2022 Aug;8(4):159.

[21] Raizah Z, Saeed A, Bilal M, Galal AM, Bonyah E. Parametric simulation of stagnation point flow of motile microorganism hybrid nanofluid across a circular cylinder with sinusoidal radius. Open Phys. 2023 Jan 25;21(1):20220205.

[22] Rehman KU, Shatanawi W, Al-Mdallal QM. A comparative remark on heat transfer in thermally stratified MHD Jeffrey fluid flow with thermal radiations subject to cylindrical/plane surfaces. Case Stud Therm Eng. 2022 Apr;32:101913.

[23] Assiri TA, Aziz Elsebaee FA, Alqahtani AM, Bilal M, Ali A, Eldin SM. Numerical simulation of energy transfer in radiative hybrid nanofluids flow influenced by second-order chemical reaction and magnetic field. AIP Adv. 2023 Mar;13(3).

[24] Upreti H, Bartwal P, Pandey AK, Makinde OD. Heat transfer assessment for Au-blood nanofluid flow in Darcy-Forchheimer

porous medium using induced magnetic field and Cattaneo-Christov model. Numer Heat Trans Part B: Fundam. 2023;84(4):1–7.
[25] Alshahrani S, Ahammad NA, Bilal M, Ghoneim ME, Ali A, Yassen MF, et al. Numerical simulation of ternary nanofluid flow with multiple slip and thermal jump conditions. Front Energy Res. 2022 Aug;10:967307.
[26] Tarakaramu N, Satya Narayana PV, Babu DH, Sarojamma G, Makinde OD. Joule Heating and Dissipation Effects on Magnetohydrodynamic Couple Stress Nanofluid Flow over a Bidirectional Stretching Surface. Int J Heat Technol. 2021 Feb;39(1).
[27] Algehyne EA, El-Zahar ER, Elhag SH, Bayones FS, Nazir U, Sohail M, et al. Investigation of thermal performance of Maxwell hybrid nanofluid boundary value problem in vertical porous surface via finite element approach. Sci Rep. 2022 Feb;12(1):2335.
[28] Qureshi ZA, Bilal S, Khan U, Akgül A, Sultana M, Botmart T, et al. Mathematical analysis about influence of Lorentz force and interfacial nano layers on nanofluids flow through orthogonal porous surfaces with injection of SWCNTs. Alex Eng J. 2022 Dec;61(12):12925–41.
[29] Duguma KA, Makinde OD, Enyadene LG. Dual solutions and stability analysis of Cu-H_2O-Casson nanofluid convection past a heated stretching/shrinking slippery sheet in a porous medium. Comput Math Methods. 2023 May;2023.
[30] Kumar P, Yadav RS, Makinde OD. Numerical study of Williamson fluid flow and heat transfer over a permeable stretching cylinder with the effects of Joule heating and heat generation/absorption. Heat Transf. 2023;52(4):3372–88.
[31] Khan A, Shah Z, Islam S, Dawar A, Bonyah E, Ullah H, et al. Darcy-Forchheimer flow of MHD CNTs nanofluid radiative thermal behaviour and convective non uniform heat source/sink in the rotating frame with microstructure and inertial characteristics. AIP Adv. 2018 Dec;8(12).
[32] Shamshuddin MD, Mabood F, Bég OA. Thermomagnetic reactive ethylene glycol-metallic nanofluid transport from a convectively heated porous surface with Ohmic dissipation, heat source, thermophoresis and Brownian motion effects. Int J Model Simul. 2022 Sep;42(5):782–96.
[33] Alqahtani AM, Bilal M, Usman M, Alsenani TR, Ali A, Mahmuod SR. Heat and mass transfer through MHD Darcy Forchheimer Casson hybrid nanofluid flow across an exponential stretching sheet. ZAMM-J Appl Math Mech/Z für Angew Math und Mech. 2023;e202200213.
[34] Duguma KA, Makinde OD, Enyadene LG. Stagnation point flow of $CoFe_2O_4$/TiO_2-H_2O-Casson nanofluid past a slippery stretching/shrinking cylindrical surface in a darcy–forchheimer porous medium. J Eng. 2023;2023.
[35] Pandey AK, Upreti H. Heat and mass transfer in convective flow of nanofluid. In Advances in Mathematical and Computational Modeling of Engineering Systems. CRC Press; 2023 Feb. p. 295–313.
[36] Prakash J, Tripathi D, Akkurt N, Shedd T. Entropy analysis of hybrid nanofluid flow over a rotating porous disk: a multivariate analysis. Spec Top Rev Porous Media: Int J. 2023;14(4).
[37] Alqahtani AM, Bilal M, Elsebaee FA, Eldin SM, Alsenani TR, Ali A. Energy transmission through carreau yasuda fluid influenced by ethylene glycol with activation energy and ternary hybrid nanocomposites by using a mathematical model. Heliyon. 2023 Apr;9(4).
[38] Mishra NK, Anwar S, Kumam P, Seangwattana T, Bilal M, Saeed A. Numerical investigation of chemically reacting jet flow of hybrid nanofluid under the significances of bio-active mixers and chemical reaction. Heliyon. 2023 Jun;e17678.
[39] Raizah Z, Alrabaiah H, Bilal M, Junsawang P, Galal AM. Numerical study of non-Darcy hybrid nanofluid flow with the effect of heat source and hall current over a slender extending sheet. Sci Rep. 2022 Sep;12(1):16280.
[40] Buongiorno J. Convective transport in nanofluids. 2006;128(3):240–50.
[41] Mishra A, Upreti H. A comparative study of Ag–MgO/water and Fe3O4–CoFe2O4/EG–water hybrid nanofluid flow over a curved surface with chemical reaction using Buongiorno model. Partial Differ Equ Appl Math. 2022 Jun;5:100322.
[42] Elattar S, Helmi MM, Elkotb MA, El-Shorbagy MA, Abdelrahman A, Bilal M, et al. Computational assessment of hybrid nanofluid flow with the influence of hall current and chemical reaction over a slender stretching surface. Alex Eng J. 2022 Dec;61(12):10319–31.
[43] Upreti H, Joshi N, Pandey AK, Rawat SK. Homogeneous–heterogeneous reactions within magnetic sisko nanofluid flow through stretching sheet due to convective conditions using Buongiorno's model. J Nanofluids. 2022 Aug;11(5):646–56.
[44] Safdar R, Gulzar I, Jawad M, Jamshed W, Shahzad F, Eid MR. Buoyancy force and Arrhenius energy impacts on Buongiorno electromagnetic nanofluid flow containing gyrotactic microorganism. Proc Inst Mech Eng Part C: J Mech Eng Sci. 2022 Sep;236(17):9459–71.
[45] Puneeth V, Anandika R, Manjunatha S, Khan MI, Khan MI, Althobaiti A, et al. Implementation of modified Buongiorno's model for the investigation of chemically reacting rGO-Fe_3O_4-TiO_2-H_2O ternary nanofluid jet flow in the presence of bio-active mixers. Chem Phys Lett. 2022 Jan;786:139194.
[46] Rasool G, Shafiq A, Hussain S, Zaydan M, Wakif A, Chamkha AJ, et al. Significance of Rosseland's radiative process on reactive Maxwell nanofluid flows over an isothermally heated stretching sheet in the presence of Darcy–Forchheimer and Lorentz forces: Towards a new perspective on Buongiorno's model. Micromachines. 2022 Feb;13(3):368.
[47] Hussain SM, Jamshed W, Safdar R, Shahzad F, Mohd Nasir NA, Ullah I. Chemical reaction and thermal characteristiecs of Maxwell nanofluid flow-through solar collector as a potential solar energy cooling application: A modified Buongiorno's model. Energy Environ. 2023 Aug;34(5):1409–32.
[48] Shoaib M, Kausar M, Nisar KS, Raja MA, Zeb M, Morsy A. The design of intelligent networks for entropy generation in Ree-Eyring dissipative fluid flow system along quartic autocatalysis chemical reactions. Int Commun Heat Mass Transf. 2022 Apr;133:105971.
[49] Bilal M, Ahmed AE, El-Nabulsi RA, Ahammad NA, Alharbi KA, Elkotb MA, et al. Numerical analysis of an unsteady, electroviscous, ternary hybrid nanofluid flow with chemical reaction and activation energy across parallel plates. Micromachines. 2022 May;13(6):874.
[50] Ahmed F, Akbar NS, Tripathi D. Numerically hydrothermal fully developed forced convective hybrid nanofluid flow through annular sector duct. Mod Phys Lett B. 2024 Mar;38(8):2450029.
[51] Goud BS, Reddy YD, Alshehri NA, Jamshed W, Safdar R, Eid MR, et al. Numerical case study of chemical reaction impact on MHD micropolar fluid flow past over a vertical riga plate. Materials. 2022 Jun;15(12):4060.
[52] Sajid T, Tanveer S, Sabir Z, Guirao JL. Impact of activation energy and temperature-dependent heat source/sink on Maxwell–Sutterby fluid. Math Probl Eng. 2020 Aug;2020:1–5.
[53] Zeeshan A, Awais M, Alzahrani F, Shehzad N. Energy analysis of non-Newtonian nanofluid flow over parabola of revolution on the

horizontal surface with catalytic chemical reaction. Heat Transf. 2021 Sep;50(6):6189–209.
[54] Shah SA, Ahammad NA, Din EM, Gamaoun F, Awan AU, Ali B. Bioconvection effects on prandtl hybrid nanofluid flow with chemical reaction and motile microorganism over a stretching sheet. Nanomaterials. 2022 Jun;12(13):2174.
[55] Wang F, Khan SA, Gouadria S, El-Zahar ER, Khan MI, Khan SU, et al. Entropy optimized flow of Darcy-Forchheimer viscous fluid with cubic autocatalysis chemical reactions. Int J Hydrog Energy. 2022 Apr;47(29):13911–20.
[56] Majee S, Shit GC. Modeling and simulation of blood flow with magnetic nanoparticles as carrier for targeted drug delivery in the stenosed artery. Eur J Mech-B/Fluids. 2020 Sep;83:42–57.
[57] Srinivas S, Reddy PB, Prasad BS. Effects of chemical reaction and thermal radiation on MHD flow over an inclined permeable stretching surface with non-uniform heat source/sink: An application to the dynamics of blood flow. J Mech Med Biol. 2014;14(5):1450067.
[58] Sharma BK, Kumawat C. Impact of temperature dependent viscosity and thermal conductivity on MHD blood flow through a stretching surface with ohmic effect and chemical reaction. Nonlinear Eng. 2021 Oct;10(1):255–71.
[59] Saeed A, Alsubie A, Kumam P, Nasir S, Gul T, Kumam W. Blood based hybrid nanofluid flow together with electromagnetic field and couple stresses. Sci Rep. 2021 Jun;11(1):12865.
[60] Misra JC, Sinha A. Effect of thermal radiation on MHD flow of blood and heat transfer in a permeable capillary in stretching motion. Heat Mass Transf. 2013;49:617–28.
[61] Dawar A, Thumma T, Islam S, Shah Z. Optimization of response function on hydromagnetic buoyancy-driven rotating flow considering particle diameter and interfacial layer effects: Homotopy and sensitivity analysis. Int Commun Heat Mass Transf. 2023 May;144:106770.
[62] Waqas H, Oreijah M, Guedri K, Khan SU, Yang S, Yasmin S, et al. Gyrotactic motile microorganisms impact on pseudoplastic nanofluid flow over a moving Riga surface with exponential heat flux. Crystals. 2022 Sep;12(9):1308.
[63] Swain K, Animasaun IL, Ibrahim SM. Influence of exponential space-based heat source and Joule heating on nanofluid flow over an elongating/shrinking sheet with an inclined magnetic field. Int J Ambient Energy. 2022 Dec;43(1):4045–57.
[64] Dawar A, Islam S, Shah Z. A comparative analysis of the performance of magnetised copper–copper oxide/water and copper–copper oxide/kerosene oil hybrid nanofluids flowing through an extending surface with velocity slips and thermal convective conditions. Int J Ambient Energy. 2022 Dec;43(1):7330–48.
[65] Alhussain ZA, Tassaddiq A. Thin film blood based Casson hybrid nanofluid flow with variable viscosity. Arab J Sci Eng. 2022 Jan;47(1):1087–94.
[66] Vedavathi N, Dharmaiah G, Venkatadri K, Gaffar SA. Numerical study of radiative non-Darcy nanofluid flow over a stretching sheet with a convective Nield conditions and energy activation. Nonlinear Eng. 2021 Jun;10(1):159–76.
[67] Souayeh B, Ramesh K. Numerical scrutinization of ternary nanofluid flow over an exponentially stretching sheet with gyrotactic microorganisms. Mathematics. 2023 Feb;11(4):981.
[68] Dey D, Chutia B. Dusty nanofluid flow with bioconvection past a vertical stretching surface. J King Saud Univ-Eng Sci. 2022 Sep;34(6):375–80.
[69] Hashim HA, Alshomrani AS, Khan M. Multiple physical aspects during the flow and heat transfer analysis of Carreau fluid with nanoparticles. Sci Rep. 2018 Nov;8(1):17402.
[70] Ahmed K, Akbar T. Numerical investigation of magnetohydrodynamics Williamson nanofluid flow over an exponentially stretching surface. Adv Mech Eng. 2021 May;13(5):16878140211019875.
[71] Hamad MA. Analytical solution of natural convection flow of a nanofluid over a linearly stretching sheet in the presence of magnetic field. Int Commun Heat Mass Transf. 2011 Apr;38(4):487–92.